Nanotoxicology, 2012; Early Online, 1–9

ISSN: 1743-5390 print / 1743-5404 online
DOI: 10.3109/17435390.2012.711862

informa
healthcare

Effect of modifying quantum dot surface charge on airway epithelial cell uptake *in vitro*

Eric Chau[1], Justin F. Galloway[3], Antoinette Nelson[1], Patrick N. Breysse[2], Denis Wirtz[3], Peter C. Searson[3], & Venkataramana K. Sidhaye[1]

[1]Departments of Medicine, Division of Pulmonary and Critical Care Medicine, Johns Hopkins University, Baltimore, MD 21224, USA, [2]Department of Environmental Health Science, Johns Hopkins University, Baltimore, MD, USA and [3]Departments of Materials Science and Engineering, Chemical and Biomolecular Engineering and Oncology and Institute of Nanotechnology, Johns Hopkins University, Baltimore, MD 21218, USA

Abstract

The respiratory system is one of the portals of entry into the body, and hence inhalation of engineered nanomaterials is an important route of exposure. The broad range of physicochemical properties that influence biological responses necessitate the systematic study to contribute to understanding occupational exposure. Here, we report on the influence of nanoparticle charge and dose on human airway epithelial cells, and show that this platform can be used to evaluate consequences of exposure to engineered nanomaterials.

Keywords: nanoparticles, quantum dots, airway epithelial cells, epithelial barrier function

Introduction

Nanoparticles are one of the key building blocks in nanoscience and the development of new nanotechnologies. As the use of nanoparticles becomes increasingly widespread, concern about the personal and public health implications of exposure to extremely small particles (<100 nm in diameter) has risen (Oberdorster et al. 2005; Nel et al. 2006). While there is much speculation about the risk of engineered nanoparticles, the biological and health effects of nanoparticle exposure in humans are not well defined. In part this is due to the broad range of physicochemical properties, such as size, shape, chemical composition and surface chemistry. As inhalation is a common and important route of exposure, we have studied the effects of nanoparticle dose and surface charge on airway epithelial cells and have found that surface charge can affect the route and time required to traverse the epithelium and alter epithelial function.

Inhalation is an important route of exposure, particularly in the occupational environment, making the lung a critical target organ and an important route of entry into the body. Between 1990 and 1999, there were over 30,000 deaths in the United States associated with occupational exposure to airborne materials (CDC website). Models indicate that the fraction of inhaled particles deposited in the respiratory system approaches 90% in the nano-size range and that a significant fraction of these particles are in the respiratory tract (head airways, trachea-bronchial and alveolar regions) (Card et al. 2008; Kreyling et al. 2006). For example, approximately 40% of inhaled 10 nm particles will deposit in the upper airways (head and trachea-bronchial regions) (ICRP 1994). Furthermore, it has been shown that the deposition fraction and deposition density (density per unit area) of inhaled particles in human bronchial airways is greatly enhanced for particles in the nano-size range compared to micron-sized particles (Winkler-Heil et al. 2007). Furthermore, the average deposition densities are highest in the upper bronchial airway (Winkler-Heil et al. 2007).

As the interface with the outside world, the airway epithelium senses information from the atmosphere and transduces it to produce both local and distant responses. The epithelial barrier allows transport of molecules such as oxygen and carbon dioxide, but restricts access of environmental antigens or pollutants to underlying tissues, and may partition signalling molecules including inflammatory mediators to one side or the other of the barrier, a function determined in part by regulation of tight junction proteins (Humlicek et al. 2007). Barrier disruption also regulates inflammatory responses to mucosal stimuli. For example, histamine increases epithelial permeability, and this effect is believed to be linked to increased airway responsiveness (Zabner et al. 2003).

Here, we report on the influence of surface charge and dose on the transport of quantum dots (QDs) across the airway epithelial barrier and on epithelial barrier function. Surface charge can affect the dispersion of particles in various media, as well as the adsorption of contaminants,

Correspondence: Venkataramana K. Sidhaye, Departments of Medicine, Division of Pulmonary and Critical Care Medicine, Johns Hopkins University, Baltimore, MD 21224, USA. E-mail: vsidhay1@jhmi.edu

(Received 21 January 2012; accepted 5 July 2012)

ions and/or biological molecules. In this study, we chose lipid-coated QD to model inhalational NP exposure. Lipid-coated nanoparticles allow us to control size, monodispersity and surface charge. Furthermore, other methods for water solubilisation usually involve pegylation that results in much larger particles. Finally, the QDs allow us to use fluorescence imaging to characterise transport.

Understanding the transport properties, nanoparticles under well-controlled conditions provide the foundations for elucidating the biochemical mechanisms. A number of studies have identified surface charge as an important determinant of biological effect, including phagocytosis, inflammation and genotoxicity (Hoet et al. 2004; Lin et al. 2008).

Materials and methods

Cell culture

Primary human bronchial epithelial cells (NHBE) (Lonza) are grown on collagen-coated inserts (Falcon) at 37○C with 5% CO_2 and maintained at an air–liquid interface for 6–9 weeks before study. The basolateral media is 50% BEBM (Lonza) media and 50% DMEM media, with Single-Quot bullet kit (Lonza) supplements as per manufacturer's suggestions. The cell membranes were labelled by incubating with 5 μL Image-IT (wheat germ agglutinin conjugated to Alexa Fluor 488, Molecular Probes) in 500 μL PBS. The transepithelial resistance (TER) was > 400 ohms when cells were used. All experiments were repeated a minimum of three times.

Specified dose of QD was suspended in 500 μL of media and added to the apical surface of the epithelial cells.

Permeability assay

Paracellular permeability of cells was assessed by the passage of 4 kD FITC-dextran across the monolayer as described previously (Sidhaye et al. 2008). Briefly, 500 μL of FITC-coupled dextran beads (4 kD, 10 mg mL^{-1}, Calbiochem, California) were added to the upper well for 20 min. About 3 mL of media was placed in the bottom well. The FITC concentration in 1 mL of the lower well was determined using a fluorometer (excitation 490 nm, detection 530 nm) and compared to static and cell-free two insert controls. The concentration was measured by fluorometry.

Chemicals

n-Hexadecylamine (HDA, 90%), trioctylphosphine oxide (TOPO, 90%), stearic acid (SA, 95%) and octadecylamine (ODA, 99%) were purchased from Sigma Aldrich (St. Louis, Missouri) and used without further purification. The precursors CdO (99.95%), $Cd(C_2H_3O_2)_2{\cdot}2H_2O$ (98%) and Zn $(C_{18}H_{35}O_2)_2$ (Tech Grade) were purchased from Sigma Aldrich and stored under ambient conditions. Bis(trimethylsilyl) sulfide ($(TMS)_2S$, purum), trioctylphosphine (TOP, 90%), Se (99.99%) and tributylphosphine (TBP, 97%) were purchased from Sigma Aldrich and stored in an argon glovebox. 1-myristoyl-2-hydroxy-*sn*-glycero-3-phosphocholine (MHPC), 1,2-distearoyl-sn-glycero-3-phosphoethanolamine-N-[methoxy (polyethylene glycol)-2000] (ammonium salt) (DSPE-PEG2k) was purchased in chloroform from Avanti Polar Lipids and stored at -20°C (Alabaster, Alabama). Hexane, methanol, chloroform and ethanol were of HPLC grade.

CdSe core synthesis

In a 250 mL reaction vessel, 2.35 mmol CdO was dissolved in 4.0 g of stearic acid (14.1 mmol) by heating to 180○C under argon. Subsequently, the heat was removed and the reaction vessel cooled to 80°C. To the flask under argon, were added 10.8 g HDA (44.7 mmol) and 4.8 g TOPO. The resealed flask was degassed at 135○C for 1 h, placed under and argon blanket and increased to 300○C. The Se precursor was prepared in an argon glovebox, by combing 11.5 mmol Se and 4 mL TBP (16.1 mmol). When the reaction vessel reached 300○C, the TBP/Se precursor was rapidly injected and the temperature lowered to 290°C. After 8 min, the heat was removed and the reaction vessel was allowed to cool to 135°C. About 25 mL of hexane was quickly injected into the reaction mixture to prevent solidification of the TOPO/HDA. The CdSe particles were extracted from the reaction mixture using centrifugation and finally precipitated using methanol. The final precipitant was resuspended in 3 mL hexane. The average QD diameter, determined from analysis of TEM images, was 6.0 nm corresponding to a peak photoluminescence of 600 nm (Park et al. 2008).The concentration of the CdSe QDs was determined using Beer's Law ($A = \varepsilon lc$) with an experimentally determined extinction coefficient for CdSe of $\varepsilon = 1397\ M^{-1}\ cm^{-1}$ at 350 nm.

CdSe electrical passivation

The CdSe QDs were passivated with a (Cd,Zn)S shell. The precursor concentrations for the shell were calculated based upon the formation of five monolayers of a shell composed of 70 mol% Zn and 30 mol% Cd on a 6.0 nm diameter CdSe QDs.

The 0.2 M Zn/Cd precursor was prepared by combining 0.485 g zinc stearate (0.78 mmol) in 3.8 mL toluene and 0.088 g $Cd(C_2H_3O_2)_2{\cdot}2H_2O$ (0.32 mmol) in 1.7 mL TOP under argon at 110○C in a sealed 20 mL glass vial for 1 h. The sulfur precursor was prepared in a glovebox under argon by combining 2 mL TOP with 0.44 mL $(TMS)_2S$ (2.1 mmol).

In a three-neck flask, 10 g TOPO (26 mmol) and 6.0 g HDA (25 mmol) were degassed for 1 h at 100°C. Next, 0.16 μmol CdSe QDs in hexane was injected into the TOPO/HDA mixture under argon and the flask quickly returned to vacuum to remove all hexane. After approximately 1 h, the flask was switched to argon and the temperature was raised to 220○C for the precursor addition. The Cd/Zn and $(TMS)_2S$ precursors were then injected slowly over 55 min and then annealed at 240○C for 15 min. The QDs were transferred to chloroform by precipitating with methanol, and re-suspended in 3 mL of chloroform at a concentration 60 μM. The concentration of the capped CdSe QDs was determined using Beer's Law with the same extinction coefficient for CdSe of $\varepsilon = 1397\ M^{-1}\ cm^{-1}$. The average thickness of the (Cd,Zn)S shell, determined from analysis of TEM images, was 0.95 nm resulting in a diameter of 7.9 nm for the core/shell QDs (Galloway et al. 2009).

30 mol% SA or ODA and 70 mol% MHPC water solubilisation

The total amount of lipids needed to functionalise the QDs was determined from the total surface area and the footprint of MHPC and SA or ODA. The radius of the CdSe/(Zn,Cd)S QDs with an HDA/TOPO inner leaflet was taken as 4.5 nm. From the molecular footprint, the diameter for MHPC was taken as 0.8 nm, and the diameter of SA and ODA were taken to be 0.5 nm (Rontu et al. 2007; Hauser et al. 1981; Didymus et al. 1995). The volume of QDs used for solubilisation was based on achieving a final concentration of QDs in water of 2.5 x 10^{-7} M. To ensure successful water solubilisation, a sevenfold-excess of lipid was used for all experiments. SA or ODA was dissolved in chloroform to give a solution of 20 mg mL^{-1} and then sonicated to ensure complete mixing. MHPC (10 mg mL^{-1}) MHPC was warmed from -20∘C to room temperature and sonicated to obtain a homogenous solution. The QD suspension, 110 μL MHPC, and 13.0 μL SA or 13.6 μL ODA solution were mixed by vigorous pipetting and then sonicated in a water bath for 20 s. Immediately after sonication, the QD+MHPC+SA or QD +MHPC+ODA solution was added dropwise to 2 mL Millipore water in a 7 mL borosilicate glass vial under vigorous stirring using a 3 x 13 mm stir bar at maximum speed. Once completely mixed, approximately 1 min, the temperature of the hot plate was raised to 90∘C. After 45–50 min, the solution was orange in colour. The solution was transferred to a centrifuge tube and spun at 8000 rpm for 3 min. The supernatant was removed using a syringe and filtered through a 200 nm, PTFE 13 mm diameter syringe filter.

20 mol% DSPE-PEG2k and 80 mol% MHPC water solubilisation

From the molecular footprint, the diameter of the DSPE-PEG2k was taken to be 0.84 nm (Nagle et al. 2000). The concentration of DSPE-PEG2k was calculated as described previously for SA or ODA, however, the diameter of QD is taken as 14 nm, which corresponds to the midpoint of the lipid bilayer. The QD suspension, 50 mg/mL DSPE-PEG2k and 10 mg/mL MHPC in chloroform were combined in a vial, mixed thoroughly by pipetting and sonicated for 20 s. Immediately after sonication, the mixture was added dropwise to 2 mL of Millipore water under vigorous stirring. After 1 min, the hotplate temperature was raised to 110∘C. At 1 h, the slightly turbid mixture was transferred to a centrifuge tube and spun at 8000 rpm for 3 min. The supernatant was then extracted and filtered through a 200 nm, PTFE 13 mm diameter syringe filter.

Characterisation

Absorbance spectra were obtained using a Varian Cary 50 UV/Vis Spectrophotometer (Agilent Technologies, Santa Clara, CA). Particle size distributions and zeta potential were obtained for QD concentrations between 1.0 x 10^{-7} and 2.3 x 10^{-7} mol L^{-1} with a volume of 0.4 mL (size distribution) or 0.7 mL (zeta potential) using a Malvern Nano Zetasizer (Worcestershire, UK). In both cases the measurement protocol was set manually to five measurements (size distribution) or six measurements (zeta potential) with automatically determined runs and no equilibration time. The particle size distributions and zeta potential were determined after discarding the first run. Error bars represent the standard error.

Immunofluorescence

Live cells were incubated with 5 μL of Image-IT (wheat germ agglutinin conjugated to Alexa Fluor 488, Molecular Probes) in 500 μL of PBS for 30 min prior to QD exposure to detect using immunofluorescence microscopy. After exposure to QDs, z-stacks were taken of cells to determine QD localisation. The microscopy resolution is limited by the fact that the cells are on inserts on an air-liquid interface and not in a culture dish.

Transmission electron microscopy

Samples were fixed in 2.5% glutaraldehyde, 3 mM $CaCl_2$, 1% sucrose in 0.1 M sodium cacodylate buffer, pH 7.2 for 1 h at room temperature. After buffer rinse, samples were postfixed in 1% osmium tetroxide in buffer (1 h) on ice in the dark. Following a DH_2O rinse, plates were stained with 2% aqueous uranyl acetate (0.22 μm filtered, 1 h, dark), dehydrated in a graded series of ethanol and embedded in Eponate 12 (Ted Pella) resin. Samples were polymerised at 60°C overnight. Thin sections, 60–90 nm, were cut with a diamond knife on the Reichert-Jung Ultracut E ultramicrotome and picked up with naked 200 mesh copper grids. Grids were stained with 2% uranyl acetate in 50% methanol and observed with a Philips CM 120 at 80 kV. Images were captured with an AMT CCD (1 x 1 K) camera.

Statistics

Statistical analysis was performed using STATA 9 (Stata Corporation) and Anova one-way analysis was primarily used to assess for statistical significance. Details specifying the numbers per experiment are specified in the figures.

Results

In this study, human airway epithelial cells grown at an air–liquid interface were used to investigate the effect of physicochemical properties on nanoparticle transport. These cells are grown on a porous support with their upper (apical) surface exposed to air and the lower (basolateral) surface to medium, allowing them to differentiate into ciliated, goblet and basal cells, forming a pseudostratified columnar epithelium that secretes an airway surface liquid (ASL) on their apical surface, similar to airway epithelial cells *in vivo* (Figure 1) (Sidhaye et al. 2008; Sidhaye et al. 2011; de Jong et al. 1994). This ASL is composed of water, salts, osmolytes and macromolecules such as mucins (Tarran 2004; Thornton & Sheehan 2004). Analysis of this type of platform has been over the past two decades and several studies support this to be a good model of *in vivo* airway epithelial cells, in terms of its ability to recapitulate the cell populations, the barrier integrity and the apico-adherens junctions found in human airways (de Jong et al. 1994), (Lin et al. 2007; Lam et al. 2011). The kinetics of transport was determined from the increase in fluorescence of the

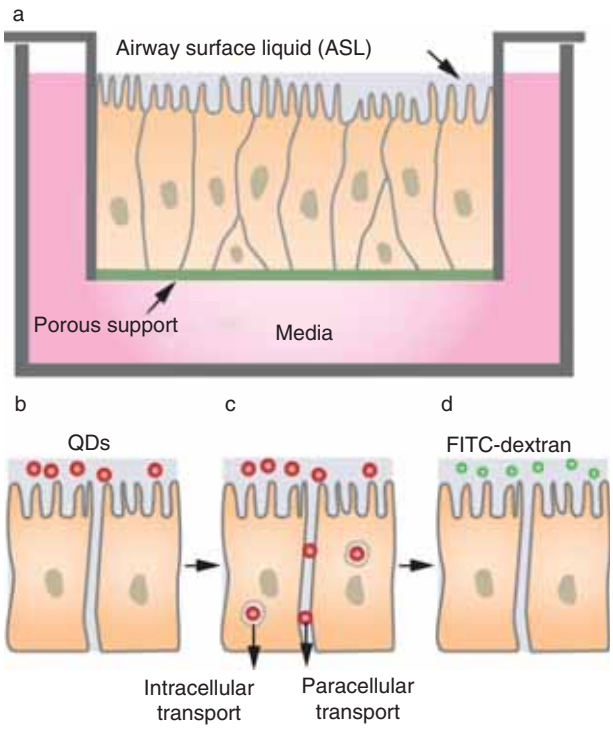

Figure 1. Schematic illustration of the platform used to study the response of the human airway epithelium to nanoparticles. (A) Human airway epithelial cells are grown on an insert such that the apical (top) surface is exposed to air and the basolateral (bottom) surface to media for 6 weeks prior to study to allow the cells to differentiate. The epithelial resistance across the monolayer is determined using a current source. (B) Quantum dots functionalised with positive or negative charge are introduced at the apical surface. (C) QDs can traverse the airway epithelium via paracellular or transcellular pathways. (D After exposures of airway epithelial cells to QDs, cells are washed and then 4 kDa FITC-dextran is placed on the apical surface and incubated for 20 min, after which the basolateral media is sampled to assess FITC concentration as a permeability assessment.

medium in the lower chamber due to transport of QDs (Figures 1B–1D). The biochemical response of the epithelium was determined using immunofluorescence microscopy, fluorescence measurements of QD transport, transepithelial electrical resistance (TER) measurements and measurements of permeability to fluorescently labelled dextran. In order to traverse the epithelium, the QDs have to first penetrate the ASL above the cells, which includes the mucus layer. Thus, this evaluation will provide insight into the ability of QDs to traverse the mucus layer, and enter and potentially cross the epithelial cells' layer as well.

CdSe/ZnS QDs were synthesised as reported previously (Park et al. 2008; Galloway et al. 2009). The QDs were water solubilised by first replacing the surfactants from synthesis with dodecanethiol (DDT) and then incubating with lipids in chloroform to form a hydrophilic outer leaflet (Galloway et al. 2011). The composition of the outer leaflet included a zwitterionic single C14 acyl chain lipid (1-myristoyl-2-hydroxy-sn-glycero-3-phosphocholine, MHPC) along with 30 mol% of Octadecylamine (ODA) and stearic acid (SA) (Figure 2A). The ODA introduces positive charge resulting in QDs with an average zeta potential of 49 mV, whereas SA introduces negative charge, resulting in QDs with an average zeta potential of –50 mV (Figure 2B).

The CdSe/ZnS core/shell QDs are 8 nm in diameter. With the DDT inner layer (≈ 1 nm) and the lipid outer leaflet (≈ 2 nm), the overall size of the QDs is expected to be about 14 nm. From dynamic light-scattering measurements, the average diameters of the ODA- and SA-modified QDs were 13.4 and 14.5 nm, respectively, in excellent agreement with the expected values (Figure 2C). The stated particle sizes are obtained from the maximum of the number density distributions. There are no additional peaks, either in number, volume or intensity distributions. Qualitatively, excessive aggregation of QDs in suspension can be seen under illumination by a black lamp, and quantitatively by a decrease in the absorbance and the appearance of a second peak in the DLS distributions. The ODA- and SA-functionalised QDs used here were selected for their stability in media. The QD suspensions were stable in media for at least 24 h (the maximum length of experiment that we have performed). From DLS measurements, there is no change in particle size after 12 h in media (Figure 1A). In addition, there is no change in the absorbance after 12 h in media indicating no aggregation or sedimentation (Figure 2D). The curve surrounding the first exciton peak at 580 nm remains unchanged after the transfer to serum indicating no change in the electronic properties of QD in serum.

In summary, the ODA- and SA-modified QDs are both about 14 nm in diameter and present an outer lipid layer with either positive or negative charge.

Workplace concentrations of nanoparticles (NP) (Davenpeck et al. 1995) on the order of 10^4 NP cm^{-3} and as high as 10^7 cm^{-3} have been reported in the literature (Demou et al. 2008). The ventilation volume for the lungs is about 6000 cm^3 per min, and the number of airway epithelial cells for an average adult is about 10^{10} (Mercer et al. 1994). An ambient concentration of 10^7 cm^{-3} corresponds to a dose of 3.6 NP per cell for an exposure of 1 h. Therefore, we chose to study doses on the order of 1, 10 or 100 NP per cell. A dose of 1 NP/cell corresponds to a high workplace exposure (10^7 cm^{-3}) for 17 min or a low workplace exposure (10^4 cm^{-3}) for seven working days. A dose of 100 NP/cell corresponds to a high workplace exposure for 3.5 working days or a low workplace exposure for 87 working weeks.

Particles can cross the epithelium by either transcellular or paracellular transport (Figure 1C). To determine the mode of entry of the QDs into the epithelial monolayer, the membranes of the airway epithelial cells were labelled with Image-IT (wheat germ agglutinin conjugated to Alexa Fluor 488, Molecular Probes). After exposure of the apical surface to QDs, live-cell confocal microscope imaging was performed to determine whether charge affected the localisation of QDs in the epithelium. Within 5 min of exposure, fluorescence imaging reveals that the QDs penetrated the epithelium (Figure 3A). For negatively charged particles, the QDs are co-localised with the membrane marker indicating that they are located between cells. In contrast, for positively charged particles, there is increased intracellular fluorescence indicating more QDs both at the apical surface of the cell, near the cilia and within the cell instead of between cells. This suggests that particle charge affects the route of transit. In EM images, in cells exposed to positively charged

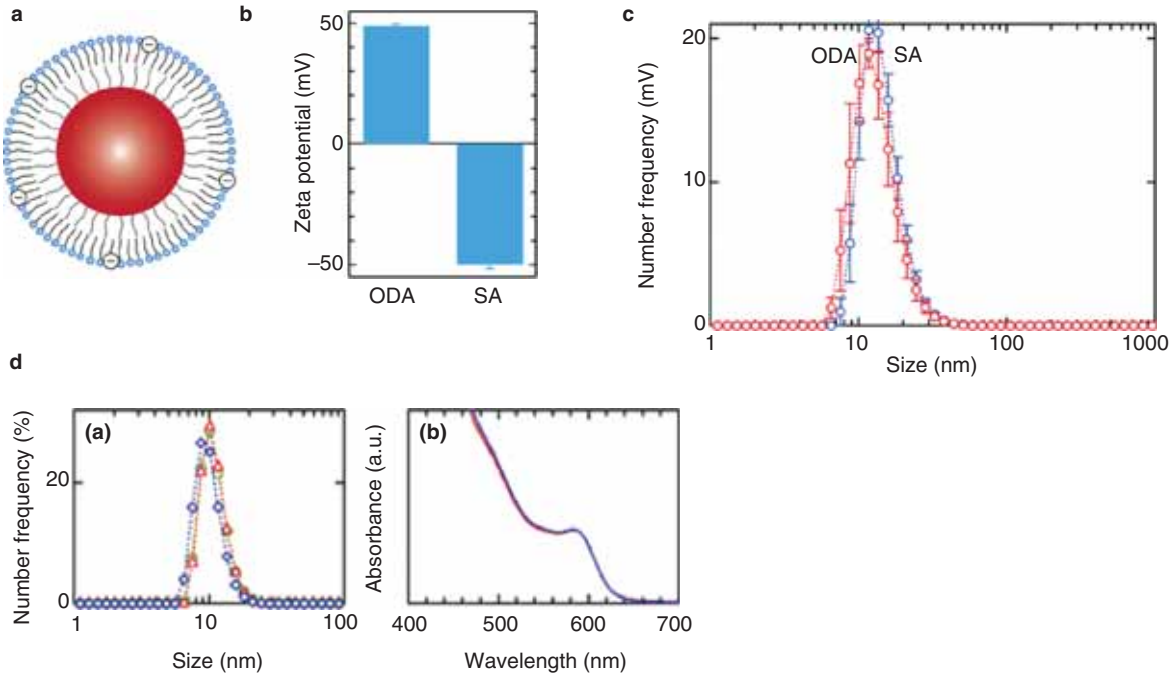

Figure 2. (A) Schematic illustration of lipid functionalised quantum dots. The outer leaflet contains 20 mol% Octadecylamine (positive charge) or stearic acid (negative charge). (B) The zeta potential was 49 mV for ODA-modified QDs and -50 mV for SA-modified QDs. (C) Particle size distributions for ODA-modified QDs (red) and SA-modified QDs (blue) (Green 2004). (D) (left) Size distributions and (right) absorbance spectra for ODA-functionalised QDs: (green) QDs in distilled water, (blue) QDs immediately after transferring to media, and (red) QDs after 12 suspension in media.

particles, there were several found within cells of different sizes (15 nm–50 nm), suggesting variable levels of aggregation. However, there were very few particles identified in cell monolayers exposed to negatively charged particles. Afew identified did in fact seem to be between cells, and were of smaller sizes (15 nm) suggesting less particle aggregation (Figure 3A). It is possible that during the monolayer processing, many of the particles between cells were washed, and therefore so few were found. Of note, in response to exposure of epithelial cells to QDs, there was no significant trypan blue staining of the monolayer, suggesting minimal cell death at the time points studies (not shown).

While other models have indicated charge-based differences in nanoparticle transit, the differences are specific to the cell studied. It has been suggested in *Hydra vulgaris* that positively charged quantum rods are endocytosed by cells (Tortiglione et al. 2009). While Dausend et al. did not find an effect of charge on nanoparticle uptake in HeLa cells (Dausend et al. 2008), their studies indicated that endocytosis of positively and negatively charged particles occurred by different mechanisms, and thereby can influence uptake in cells depending on which mechanisms predominate. Therefore, uptake of charged particles can be cell specific, and our platform provides data about how the respiratory airway epithelium responds to inhaled nanoparticles. While there is data in the lower alveolar epithelium (Fazlollahi et al. 2011; Fazlollahi et al, 2011; Kim et al. 2010; Yacobi et al. 2008, 2009, 2007), the airway epithelium has a higher paracellular permeability (Widdicombe J 1997), and transport could be substantially altered. The mechanisms dictating these routes are unknown. In addition, it is not clear whether negatively charged QDs are primarily transported via the paracellular pathway due to exclusion from a transcellular pathway, or due to selectivity by proteins mediating cell–cell contacts. Unlike the transcellular route, which has both active and passive processes regulating transport, paracellular transport is believed to have only passive processes driven by the gradients created by transcellular transport mechanisms (Anderson & Van Itallie 1995). The major barrier in the paracellular route is the tight junction, which varies in ion selectivity. At physiological pH, most tight junctions are thought to be slightly cation selective (Colegio et al. 2003), potentially contributing to the increase in negative QDs between cells.

Since the QDs are photoluminescent, we can determine whether they cross the epithelial barrier by sampling the fluorescence in the basolateral medium (Figure 3B). Within 30 min of exposure to QDs there was evidence of increased fluorescence in the basolateral medium of cells incubated with both positively and negatively charged particles, indicating that both crossed the epithelial barrier. After 30 min incubation with QDs, the amount of negatively charged particles in the basolateral medium was relatively independent of dose. In contrast, the amount of positively charged particles was significantly higher at doses of 10 and 100 NP/cell compared to negatively charged particles. Since the negatively charged particles are preferentially localised at the cell–cell junctions, this suggests that either transcellular transport in faster than paracellular transport or, more likely, that the capacity for storing QDs in the paracellular regions is high resulting in a delay in transport into the basolateral media. The fluorescence does not increase linearly with

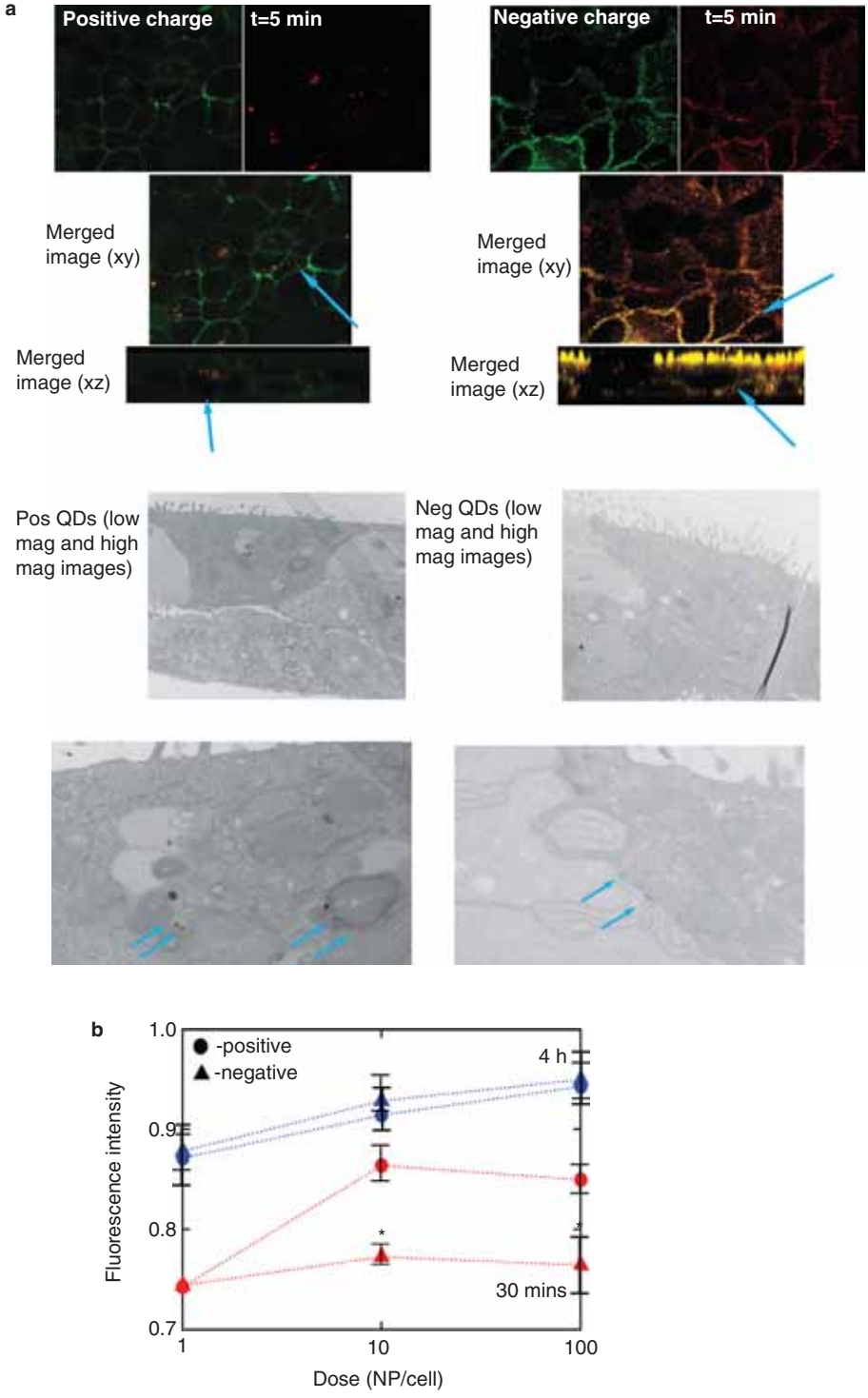

Figure 3. (A) After 5 min exposure, QDs penetrate the epithelium. Fluorescence images for airway epithelial cells 5 min after incubating with a dose of 10 NP/cell. (Green) Cell membrane, (red) QDs. After 5 min exposure, the majority of the negatively charged QDs are located at the cell–cell junctions, whereas the majority of the positively charged QDs are located with the cells. (B) By measuring the fluorescence in the basolateral media we can assess QD transport across the epithelial barrier. Both negatively and positively charged particles cross the epithelial barrier. (Bars represent standard error (SE), $n = 3$ for each dose; Anova one-way ($p < 0.025$)).

dose, implying that there is a significant fraction of QDs within the epithelial layer. After 4 h incubation, the amount of QDs increased approximately linearly with dose, and was independent of charge, suggesting that the amount of QDs in the epithelial layer has saturated and that the global transport kinetics have reached a steady state, independent of charge.

One of the fundamental features of the airway epithelium is its barrier properties. The epithelial barrier is the first line of defence preventing access of inhaled particles to subepithelial tissues (Gabrielson et al. 1994; Yu et al. 1994; Yu et al. 1994; Rothen-Rutishauser et al. 2008). However, the epithelium also serves to segregate the apical and basal compartments (Humlicek et al. 2007), (Sidhaye et al.

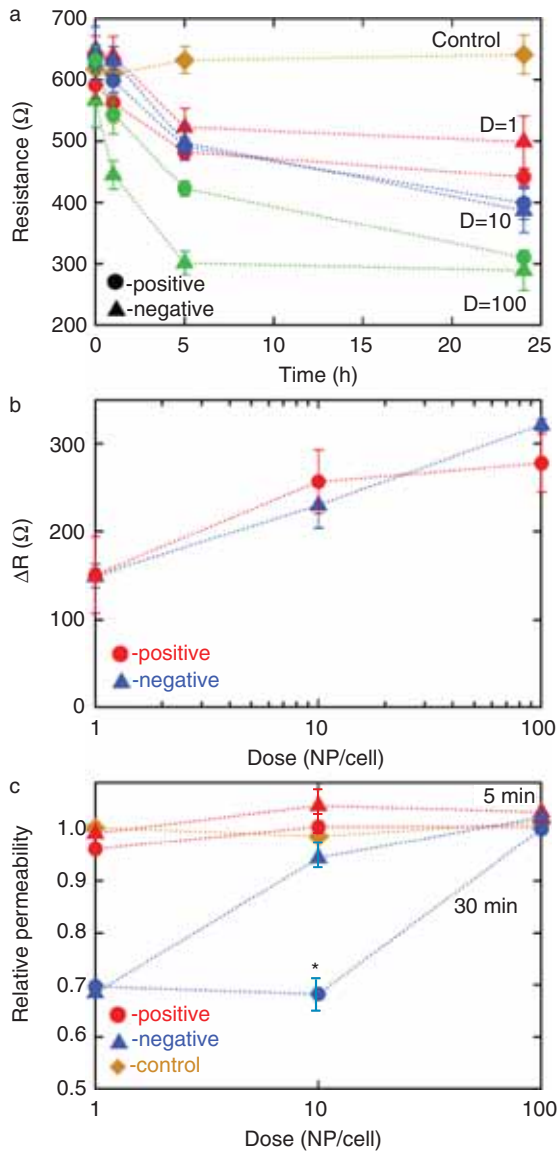

Figure 4. Nanoparticle exposure results in altered airway epithelial barrier function. (A) TER versus time for airway epithelial cells incubated with 1, 10 or 100 NP/cell. Both positively and negatively charged QDs decrease TER in a dose-responsive fashion. The control represents incubation with buffer only. (Bars represent standard error (SE) with at least three independent experiments) (B) The change in TER after 24 h increases exponentially with dose, independent of charge. (C) After exposure to QD, the 4 kD FITC-dextran was placed in the apical chamber and after incubating for 20 min (37°C) the basolateral media was sampled to assess fluorescence. In response to 30 min of exposure to a very low exposure of QD (in the order of 1 NP/cell), there was a significant decrease in paracellular permeability. (Bars represent standard error (SE), $n = 3$ per condition; Anova one-way ($p < 0.025$)).

2011; Winter et al. 2006) so that regulation of epithelial barrier properties can influence cell signalling (Humlicek et al. 2007; Sidhaye et al. 2011). In order to determine if QD charge could affect airway epithelial barrier function, we measured TER using two probe electrodes inserted on either side of the barrier (Figure 4A). The TER decreased for both positively and negatively charged particles in a dose-responsive fashion, indicating that exposure to QDs compromises barrier function. The largest change in TER occurred between 1 and 5 h of exposure, consistent with the fluorescence results shown in Figure 3B. In particular, even a very low exposure of QD, at a concentration of approximately 1 NP/cell was sufficient to cause a significant decrease in TER after 5 h exposure. The change in resistance after 24 h exposure increases exponentially with dose (Figure 4B), independent of charge.

Previous studies have concluded that there is no correlation between change in TER and solute flux,(McCarthy et al. 1996) and hence we assessed the effects of QDs on paracellular permeability by measuring the barrier permeability to 4 kDa FITC-dextran (Figure 4C). The TER measurements described above are sensitive to ionic transport and show that QD exposure decreases the resistance corresponding to an increase in ionic transport. The hydrodynamic diameter of dextran is about 2.5 nm (Armstrong et al. 2004), an order of magnitude larger than Na^+, K^+ and Cl^-, and hence the dextran permeability experiments probe larger length scales.

After incubation with QDs for different times, the fluorescently labelled dextran was injected into the ASL. Dextran transport across the airway epithelial cells was determined from fluorescence measurements of the medium from the basolateral chamber. After 5 min of exposure, there is no change in permeability compared to a barrier that had not been previously exposed to QDs. After 30 min of exposure, however, the permeability decreased with decreasing dose. At this larger length scale, exposure to QDs at low dose decreases dextran permeability after 30 min, whereas exposure to large doses has no effect. While this result is unexpected, one potential explanation is that the epithelial response to low doses resulting in enhanced barrier function is overwhelmed at higher doses. This is in contrast to previous work where we showed that initial exposure to micron-sized particles can result in decreases in permeability without dose dependence (Sidhaye et al. 2011).

Discussion

Quantum dots are a model system in which we are able to carefully control the size, surface chemistry, charge and monodispersity, to study the ability of nano-sized particles to cross the airway epithelial barrier as well their effects on that barrier. We have shown that QDs can be taken up and cross the human airway epithelial barrier. The lung epithelium, both airway and alveolar, is poised to be exposed to inhaled particles, and it has been estimated that there is significant deposition in the airways (ICRP 1994). Of note, it has been calculated that the airway epithelial barrier is more permeable than the alveolar barrier (Widdicombe J 1997), and therefore mechanisms of transport could be of great significance in airway epithelial cells. Studies have shown that charged particles can traverse the alveolar epithelium, primarily transcellularly (Fazlollahi et al. 2011; Fazlollahi et al, 2011; Kim et al. 2010; Yacobi et al. 2008, 2009, 2007). Published studies, such as those by Yacobi et al.(Yacobi et al. 2009) have considered nanoparticle transport through the alveolar epithelium, and have shown that both positively and negatively charged particles traverse transcellularly, though at different rates. Our study adds to the literature by showing that nanoparticle

transport is cell-type dependent, and charge dictates both rate and route of particle transport in airway epithelial cells. Perhaps the difference in barrier properties between the alveoli and airways could account for the differences found in our study of airway epithelium.

The charge of the particle dictates the path by which the QDs traverse the airway epithelial barrier, with positively charged QDs transported by an intracellular pathway and negatively charged QDs transported via a paracellular pathway. Exposure to positively and negatively charged QDs resulted in an exponential decrease in TER with increasing dose. Transepithelial resistance can be altered by many things, including changes in cell–cell contacts resulting in altered bulk flow between cells, as well as changes in ionic transport due to altered channel expression or function. Conversely, exposure to QDs resulted in a decrease in permeability to an electrically neutral probe (dextran) at low doses but no change in permeability at higher doses. These combined results suggest that the change in resistance is not due to altered cell–cell contacts, which would be reflected in altered dextran permeability, but some change in ionic transport. More research is needed to evaluate the mechanism and significance of changes in barrier function. These results show that small nanoparticles can cross the barrier formed by airway epithelial cells and that transport is dependent on charge, dose and time. In addition to crossing the epithelium, these nanoparticles also altered airway epithelial function as determined by decreases in paracellular permeability. We believe these studies indicate that our platform allows us to understand what aspects of NPs confer toxicity to inform environmental policy. In addition, this system could potentially allow for identification of new uses of NPs to specifically target epithelial cells.

Acknowledgements

This work was supported by the FAMRI Young Investigator Award and K08HL085763. JG and PS acknowledge support from NIH U54CA151838. Support for PNB was provided by NSF 0837946.

Declaration of interest

The authors report no conflicts of interest. The authors alone are responsible for the content and writing of the paper.

References

Anderson JM, Van Itallie CM. 1995. Tight junctions and the molecular basis for regulation of paracellular permeability. Am J Physiol 269(4 Pt 1):G467–G475.

Armstrong JK, Wenby RB, Meiselman HJ, Fisher TC. 2004. The hydrodynamic radii of macromolecules and their effect on red blood cell aggregation. Biophys J 87(6):4259–4270.

Card JW, Zeldin DC, Bonner JC, Nestmann ER. 2008. Pulmonary applications and toxicity of engineered nanoparticles. Am J Physiol Lung Cell Mol Physiol 295(3):L400–L411.

Colegio OR, Van Itallie C, Rahner C, Anderson JM. 2003. Claudin extracellular domains determine paracellular charge selectivity and resistance but not tight junction fibril architecture. Am J Physiol Cell Physiol 284(6):C1346–C1354.

Dausend J, Musyanovych A, Dass M, Walther P, Schrezenmeier H, Landfester K, et al. 2008. Uptake mechanism of oppositely charged fluorescent nanoparticles in HeLa cells. Macromol Biosci 8 (12):1135–1143.

Davenpeck KL, Chrest FJ, Sterbinsky SA, Bickel CA, Bochner BS. 1995. Carboxyfluorescein diacetate labeling does not affect adhesion molecule expression or function in human neutrophils or eosinophils. J Immunol Methods 188(1):79–89.

de Jong PM, van Sterkenburg MA, Hesseling SC, Kempenaar JA, Mulder AA, Mommaas AM, et al. 1994. Ciliogenesis in human bronchial epithelial cells cultured at the air-liquid interface. Am J Respir Cell Mol Biol 10(3):271–277.

Demou E, Peter P, Hellweg S. 2008. Exposure to manufactured nanostructured particles in an industrial pilot plant. Ann Occup Hyg 52 (8):695–706.

Didymus JM, Mann S, Benton WJ, Collins IR. 1995. Interaction of Poly(Alpha,Beta-Aspartate) with Octadecylamine Monolayers - Adsorption Behavior and Effects on Caco3 Crystallization. Langmuir 11(8):3130–3136.

Fazlollahi F, Angelow S, Yacobi NR, Marchelletta R, Yu AS, Hamm-Alvarez SF, et al. 2011. Polystyrene nanoparticle trafficking across MDCK-II. Nanomedicine 7(5):588–594.

Fazlollahi F, Sipos A, Kim YH, Hamm-Alvarez SF, Borok Z, Kim KJ, et al. 2011. Translocation of PEGylated quantum dots across rat alveolar epithelial cell monolayers. Int J Nanomedicine 6:2849–2857.

Gabrielson EW, Yu XY, Spannhake EW. 1994. Comparison of the toxic effects of hydrogen peroxide and ozone on cultured human bronchial epithelial cells. Environ Health Perspect 102(11):972–974.

Galloway JF, A W, Lee KH, Park J, Devreotes P, Peter C, et al. 2011. Devreotes, and Peter C. Searson (2011) Quantitative characterization of the lipid encapsulation of quantum dots for biomedical applications. Nanomedicine: Nanotechnol Biol Med; Under review.

Galloway JF, Park J, Lee KH, Wirtz D, Searson PC. 2009. Exploiting Nucleation and Growth in the Synthesis and Electrical Passivation of CdSe Quantum Dots. Sci Adv Mater 1(1):1–8.

Galloway JF, P J, Lee HH, Wirtz D, Searson 2009. Searson (2009) Exploiting nucleation and growth in the synthesis and electrical passivation of CdSe quantum dots. Sci Adv Mater 1:93–100.

Green AS. 2004. Modelling of peak-flow wall shear stress in major airways of the lung. J Biomech 37(5):661–667.

Hauser H, Pascher I, Pearson RH, Sundell S. 1981. Preferred Conformation and Molecular Packing of Phosphatidylethanolamine and Phosphatidylcholine. Biochimica Et Biophysica Acta 650(1):21–51.

Hoet PH, Bruske-Hohlfeld I, Salata OV. 2004. Nanoparticles - known and unknown health risks. J Nanobiotechnology 2(1):12.

Humlicek AL, Manzel LJ, Chin CL, Shi L, Excoffon KJ, Winter MC, et al. 2007. Paracellular permeability restricts airway epithelial responses to selectively allow activation by mediators at the basolateral surface. J Immunol 178(10):6395–6403.

ICRP. Human respiratory tract model for radiological protection. Oxford: ICRP Publication Oxford 1994.

Kim YH, Fazlollahi F, Kennedy IM, Yacobi NR, Hamm-Alvarez SF, Borok Z, et al. 2010. Alveolar epithelial cell injury due to zinc oxide nanoparticle exposure. Am J Respir Crit Care Med 182(11): 1398–1409.

Kreyling WG, Semmler-Behnke M, Moller WJ. 2006. Ultrafine particle-lung interactions: does size matter?. Aerosol Med 19(1):74–83.

Lam E, Ramke M, Groos S, Warnecke G, Heim A. 2011. A differentiated porcine bronchial epithelial cell culture model for studying human adenovirus tropism and virulence. J Virol Methods 178(1-2): 117–123.

Lin H, Li H, Cho HJ, Bian S, Roh HJ, Lee MK, et al. 2007. Air-liquid interface (ALI) culture of human bronchial epithelial cell monolayers as an in vitro model for airway drug transport studies. J Pharm Sci 96(2):341–350.

Lin P, Chen JW, Chang LW, Wu JP, Redding L, Chang H, et al. 2008. Computational and ultrastructural toxicology of a nanoparticle, Quantum Dot 705, in mice. Environ Sci Technol 42(16):6264–6270.

McCarthy KM, Skare IB, Stankewich MC, Furuse M, Tsukita S, Rogers RA, et al. 1996. Occludin is a functional component of the tight junction. J Cell Sci 109(Pt 9):2287–2298.

Mercer RR, Russell ML, Roggli VL, Crapo JD. 1994. Cell number and distribution in human and rat airways. Am J Respir Cell Mol Biol 10(6):613–624.

Nagle JF, Tristram-Nagle S. 2000. Structure of lipid bilayers. Biochimica et Biophys Acta-Reviews Biomemb 1469(3):159–195.

Nel A, Xia T, Madler L, Li N. 2006. Toxic potential of materials at the nanolevel. Science 311(5761):622–627.

Oberdorster G, Oberdorster E, Oberdorster J. 2005. Nanotoxicology: an emerging discipline evolving from studies of ultrafine particles. Environ Health Perspect 113(7):823–839.

Park J, Lee KH, Galloway JF, Searson PC. 2008. Synthesis of Cadmium Selenide Quantum Dots from a Non-Coordinating Solvent: Growth Kinetics and Particle Size Distribution. J Phys Chem C 112 (46):17849–17854.

Rontu N, Vaida V. 2007. Miscibility of perfluorododecanoic acid with organic acids at the air-water interface. J Phy Chem C 111(27): 9975–9980.

Rothen-Rutishauser B, Blank F, Muhlfeld C, Gehr P. 2008. In vitro models of the human epithelial airway barrier to study the toxic potential of particulate matter. Expert Opin Drug Metab Toxicol 4 (8):1075–1089.

Sidhaye V, Schweitzer K, Caterina MJ, Shimoda LA, King LS. 2008. Shear stress regulates AQP5 and airway epithelial barrier function. Proc Natl Acad Sci USA 105(9):3345–3350.

Sidhaye VK, Chau E, Breysse P, King LS. 2011. Septin-2 Mediates Airway Epithelial Barrier Function in Physiologic and Pathologic Conditions. Am J Respir Cell Mol Biol 45(1):120–126.

Tarran R. 2004. Regulation of airway surface liquid volume and mucus transport by active ion transport. Proc Am Thorac Soc 1(1):42–46.

Thornton DJ, Sheehan JK. 2004. From mucins to mucus: toward a more coherent understanding of this essential barrier. Proc Am Thorac Soc 1(1):54–61.

Tortiglione C, Quarta A, Malvindi MA, Tino A, Pellegrino T. 2009. Fluorescent nanocrystals reveal regulated portals of entry into and between the cells of Hydra. PLoS One 4(11):e7698.

Widdicombe J. Airway and alveolar permeability and surface liquid thickness: theory. J Appl Physiol 1997:82(1):3–12.

Winkler-Heil R, Hofmann W, Marsh J, Birchall A. 2007. Comparison of radon lung dosimetry models for the estimation of dose uncertainties. Radiat Prot Dosimetry 127(1-4):27–30.

Winter MC, Shasby SS, Ries DR, Shasby DM. 2006. PAR2 activation interrupts E-cadherin adhesion and compromises the airway epithelial barrier: protective effect of beta-agonists. Am J Physiol Lung Cell Mol Physiol 291(4):L628–L635.

Yacobi NR, Demaio L, Xie J, Hamm-Alvarez SF, Borok Z, Kim KJ, et al. 2008. Polystyrene nanoparticle trafficking across alveolar epithelium. Nanomedicine 4(2):139–145.

Yacobi NR, Malmstadt N, Fazlollahi F, DeMaio L, Marchelletta R, Hamm-Alvarez SF, et al. 2009. Mechanisms of alveolar epithelial translocation of a defined population of nanoparticles. Am J Respir Cell Mol Biol 42(5):604–614.

Yacobi NR, Phuleria HC, Demaio L, Liang CH, Peng CA, Sioutas C, et al. 2007. Nanoparticle effects on rat alveolar epithelial cell monolayer barrier properties. Toxicol In Vitro 21(8):1373–1381.

Yu XY, Schofield BH, Croxton T, Takahashi N, Gabrielson EW, Spannhake EW. 1994. Physiologic modulation of bronchial epithelial cell barrier function by polycationic exposure. Am J Respir Cell Mol Biol 11(2):188–198.

Yu XY, Takahashi N, Croxton TL, Spannhake EW. 1994. Modulation of bronchial epithelial cell barrier function by in vitro ozone exposure. Environ Health Perspect 102(12):1068–1072.

Zabner J, Winter M, Excoffon KJ, Stoltz D, Ries D, Shasby S, et al. 2003. Histamine alters E-cadherin cell adhesion to increase human airway epithelial permeability. J Appl Physiol 95(1):394–401.